PCCP

ROYAL SOCIETY OF CHEMISTRY

PAPER

View Article Online
View Journal | View Issue

Cite this: *Phys. Chem. Chem. Phys.*, 2025, **27**, 21283

Modeling CH_3SOH–aromatic complexes to probe cysteine sulfenic acid–aromatic interactions in proteins

Esam A. Orabi [ab] and Ann M. English *[a]

Cysteine sulfenic acid (CysOH), formed on oxidation of Cys residues, is an intermediate in the catalytic cycles of numerous antioxidant enzymes and participates in oxidative-stress sensing and redox signaling. Proteins control CysOH reactivity in part by its interactions with aromatic residues. To characterize such interactions, we performed extensive *ab initio* quantum mechanical calculations with MP2(full)/6-311++G(d,p) on complexes of CH_3SOH as a CysOH model with side-chain models for Phe (toluene), Trp (3-methylindole), Tyr/Tyr^- (4-methylphenol/4-methylphenolate) and His/$HisH^+$ (4-methylimidazole/4-methylimidazolium) residues. The gas-phase global minima conformers extracted from the 67 aromatic complexes found exhibit binding energies of ~−5 to −25 kcal mol^{-1}. In the neutral CH_3SOH–aromatics, the center oxidized is the stronger H-bond donor, which varies with the geometry of the complex as does the ionization potential (IPV). While CH_3SOH (IPV = 9.20 eV) is exclusively oxidized when complexed to 4-methylimidazolium (IPV = 14.64 eV), the phenol ring is oxidized in all CH_3SOH complexes with 4-methylphenolate (IPV = 3.31 eV). To perform molecular dynamics (MD) simulations of the aqueous complexes, a potential model was optimized for CH_3SOH and calibrated for its interactions with the aromatic ions. The MD simulations reveal that in bulk water the S atom preferentially adopts en-face or intermediate binding geometry with binding free energies of ~−0.6, −2.5 and −5 kcal mol^{-1} for the neutral, imidazolium and phenolate complexes, respectively. Overall, the gas-phase and aqueous CH_3SOH complexes are 40–170% more stable and 0–40% less stable, respectively, than their CH_3SH counterparts. Exceptionally, aqueous 4-methylphenolate binds CH_3SOH ~50% more tightly than CH_3SH due to strong σ-type O–H···O_{ar} H-bond bonding. Examination of a subset of CysOH–aromatics from the Protein Data Bank highlight their role in CysOH formation and stabilization in proteins.

Received 4th August 2025,
Accepted 17th September 2025

DOI: 10.1039/d5cp02976g

rsc.li/pccp

Introduction

Although Cys comprises only ~2% of all residues in proteins,[1] its versatile redox chemistry is crucial for function. The oxidation number of the S atom can vary between −2 and +6 allowing the thiol group to be converted to a sulfenic, sulfinic and sulfonic acid, a sulfenamide, persulfide, disulfide, and *S*-nitrosothiol. These redox changes are induced by reactive nitrogen, oxygen, or sulfur species, making Cys residues key regulators in redox homeostasis and signaling.[2,3]

Cys sulfenic acid (CysOH) is among the redox-reversible Cys oxoforms. In fact, the reversible oxidation of Cys to CysOH commonly regulates protein function, catalysis and signalling.[2] For example, CysOH is involved in protein tyrosine phosphatase (PTP) signal transduction pathways,[4] activation and function of T-cells,[5] and redox-switching to regulate kinase activity.[6]

Under oxidative stress, which is linked to neurodegeneration and cancer pathogenesis,[7] CysOH is often the first Cys oxidation product detected. Its susceptibility to further oxidation and the end products formed depend not only on the oxidant but also on the protein microenvironment such as the polarity of neighbouring residues and solvent accessibility.[2] Furthermore, we have reported previously that charge transfer between aromatic residues and Cys (or Met) also impacts the redox properties of both.[8,9] In fact, recurrent noncovalent S–aromatic interactions between Cys or Met and Phe, Tyr, Trp or His contribute significantly to protein stability and function.[10–15] Towards characterizing CysOH–aromatic interactions and their influence on CysOH redox properties, here we investigate gas-

[a] *Center for Research in Molecular Modeling (CERMM), Quebec Network for Research on Protein Function, Engineering, and Applications (PROTEO), and Department of Chemistry and Biochemistry, Concordia University, 7141 Sherbrooke Street West, Montreal, Quebec H4B 1R6, Canada. E-mail: ann.english@concordia.ca; Tel: +1-514-848-2424ext3378*
[b] *Current address: Laboratory of Membrane Proteins and Structural Biology, Biochemistry and Biophysics Center, National Heart, Lung, and Blood Institute, National Institutes of Health, Bethesda, MD, USA*

phase and aqueous model complexes of methanesulfenic acid (CH_3SOH) with toluene, 3-methylindole, 4-methylphenol/4-methylphenolate and 4-methylimidazole/4-methylimidazolium as proxies for the side chains of Phe, Trp, Tyr/Tyr^- and His/$HisH^+$ residues, respectively.

We performed *ab initio* quantum mechanical (QM) calculations to obtain geometries and interaction energies of the gas-phase CH_3SOH–aromatic and CH_3SOH–H_2O complexes. A new additive potential model was developed for CH_3SOH and used together with the CHARMM36 all-atom additive force field (FF)[16] for the aromatic residues and the CHARMM-compatible TIP3P model for water[17,18] in molecular dynamics (MD) simulations to evaluate the geometry and stability of the CH_3SOH–aromatics in bulk water. Our detailed analysis of the properties of the CH_3SOH–aromatic complexes provides a comprehensive data set that expands our profiling of the S–aromatic motif in proteins. Comparison with our previous investigations on Cys–aromatic interactions[8,9] sheds new light on how S-aromatic interactions influence CysOH formation and redox stability and thereby the impact of Cys oxidation on protein structure and function.

Computational methods

Ab initio calculations

QM calculations were performed with the Gaussian 09 program.[19] The geometry of methanesulfenic acid (CH_3SOH) and a relaxed scan of its CSOH dihedral angle φ_{CSOH} between 0° and 180° in 5°-increments were calculated with MP2(full)/6-311++G(d,p) and MP2(full)/6-311++G(3df,3pd). The geometry of CH_3SOH complexes with water, toluene, 3-methylindole, 4-methylphenol, 4-methylphenolate, 4-methylimidaole and 4-methylimidazolium were optimized with MP2(full)/6-311++G(d,p) without constraints by initially placing the interacting ligands at various relative orientations while considering all possible σ- and π-type H-bonding as well as S–π and O–π interactions. For the 7 binary complexes examined, over 300 structures were optimized and these converged to 69 energy minima structures (no imaginary frequencies). The coordinates of the 69 unique structures are provided in the SI and their geometries are reported in Fig. 2 and SI Fig. S1–S7. The counterpoise (CP) procedure of Boys and Bernardi[20] was used to correct the interaction energies for basis set superposition error (BSSE) and both uncorrected (E) and corrected values (E^{CP}) are reported. However, to benchmark the results reported here, interaction energies of the seven global minimum conformers were also calculated at their MP2(full)/6-311++G(d,p) geometries using the B3LYP[21] and M06-2X[22] density functional and the MP2(full) and CCSD(T) methods with the 6-311++G(d,p), 6-311++G(3df,3pd), and aug-ccpVQZ basis sets.

The impact of complexation on the redox properties of the interacting ligands is investigated by comparing the calculated vertical ionization potentials (IPV) of the isolated ligands and the complexes, measuring the degree of charge transfer between the ligands by natural bond order (NBO) analysis, and localizing radical sites in the complexes following electron loss.[9,23,24]

The default FF described below underestimates the interaction energies of the charged aromatics relative to the MP2(full)/6-311++G(d,p) values. Hence, rigid-monomer potential energy curves (PECs) were generated for two conformers of CH_3SOH–4-methylimidazolium and CH_3SOH–4-methylphenolate by scanning the distance from 3.0 to 10.0 Å between the S atom and the aromatic ring centroid in 0.1-Å increments. The geometry of the interacting fragments and their relative orientations are fixed to those of the optimized conformers and the PECs are corrected for BSSE and later used to calibrate the FF for the ionic complexes.

Molecular mechanics (MM) calculations

Small CH_3SOH–aromatic complexes are amenable to high-level QM calculations in the gas phase, but such calculations become prohibitive for the solvated complexes. MM calculations are typically performed instead and were implemented here with CHARMM[25] using the CHARMM36 all-atom additive FF[16] for the aromatic compounds, the CHARMM-compatible TIP3P model for water,[17,18] and our new model developed in the next section for CH_3SOH. Interaction energies of the CH_3SOH complexes (E^{MM} and $E^{MM,opt}$) at various points along the PECs were calculated with the FF as the difference in energy between the complex and its isolated constituents while maintaining their *ab initio* geometries.

FF Development for CH_3SOH. The potential energy function $U(r)$ used for the CH_3SOH additive model is given by:[25]

$$\begin{aligned} U(r) \;=\; & \sum_{\text{bonds}} K_b(b-b_0)^2 + \sum_{\text{angles}} K_\theta(\theta-\theta_0)^2 \\ & + \sum_{\text{Urey-Bradley}} K_S(S-S_0)^2 + \sum_{\text{dihedrals}} K_\varnothing(1+\cos(n\varnothing-\delta)) \\ & + \sum_{\text{non bonded}} \left\{ \epsilon_{ij}\left[\left(\frac{R_{\min,ij}}{r_{ij}}\right)^{12} - 2\left(\frac{R_{\min,ij}}{r_{ij}}\right)^{6}\right] + \frac{q_i q_j}{r_{ij}} \right\} \end{aligned} \tag{1}$$

where b refers to CH, CS, SO, and OH bond distances; θ to the HCH, HCS, CSO, and SOH valence angles; S to HH distances (of the CH_3 group) and SH distance (of the SOH group), Φ to the HCSO and CSOH dihedral angles. The 0 subscript designates equilibrium values; K_r, K_θ, K_S and K_Φ are the corresponding force constants, and parameters n and δ in the dihedral term represent the periodicity and phase angle, respectively. The nonbonded term in eqn 1 describes nonbonded van der Waals and electrostatic interactions between atoms i and j *via* (6–12) Lennard-Jones (LJ) and Coulomb terms. The partial charges on atoms i, j are q_i, q_j, while r_{ij} is the distance between nonbonded atoms i and j. The minimum interaction radius $R_{\min,ij}$ and the well-depth ϵ_{ij} in the LJ potential are determined from individual LJ parameters for atoms i and j using the Lorentz–Berthelot combination rules:

$$\epsilon_{ij} = \sqrt{\epsilon_i \times \epsilon_j} \quad \text{and} \quad R_{\min,ij} = \frac{R_{\min,i} + R_{\min,j}}{2} \tag{2}$$

An initial guess of the FF parameters of CH_3SOH was performed using the CHARMM general FF (CGenFF) online

tool.[26] Except for the LJ parameters, other parameters were refined to reduce large deviations from *ab initio* calculations or large penalties assigned by the CGenFF. Parameters b_0, θ_0, S_0 and Φ_0 were obtained from geometry optimization of CH_3SOH with MP2(full)/6-311++G(3df,3pd); K_r, K_θ, K_S and K_Φ are adjusted to reproduce the vibrational frequencies calculated at the same level and scaled by 0.945. Partial charges on the CH_3 atoms ($q_H = 0.09e$ and $q_C = -0.15e$) are set to those of dimethyl sulfoxide (CH_3SOCH_3) in the CGenFF and q_S is set to $-0.12e$ to give a neutral CH_3S fragment. To maintain a neutral OH group, q_H is set to $-q_O$ with charges set to reproduce the dipole moment of gaseous CH_3SOH calculated at the same level. The dihedral parameters n and δ for the HCSO angle are assigned the values predicted by the CGenFF while those of the CSOH angle are set to yield torsional potentials in good agreement with the QM calculations. Our optimized FF for CH_3SOH is reported in the SI.

FF optimization for CH_3SOH interactions

The default FF gives interaction energies for the CH_3SOH complexes of the four neutral aromatics and H_2O in good agreement with the E^{CP} values calculated with MP2(full)/6-311++G(d,p) but significantly underestimates the stabilities of the charged complexes. Optimization of the FF for CH_3S–4-methylimidazolium and CH_3SOH–4-methylphenolate follows previously reported procedures.[8,9,23,24,27–32] In particular, ϵ_{Oj} and $R_{min,Oj}$, the pair-specific LJ parameters referring to the O atom of CH_3SOH (O) and an imidazolium N or the phenolate O atom (j) in the nonbonded van der Waals energy term, are optimized to reproduce the ten lowest E^{CP} values covering a range of 0.9 Å in 0.1-Å increments in the PEC of each complex. The optimized LJ parameters were input in the NBFIX section of the CHARMM parameter file to override the default values from the Lorentz–Berthelot combination rules.

We have previously shown that the default FF reasonably reproduces the properties of H_2O–aromatics except for overestimating the stability of H_2O–4-methylphenolate.[8,9] Thus, previously optimized pair-specific LJ parameters[8] were used in MD simulations of this complex in water.

Molecular dynamics. MD simulations were performed in a box of 500 water molecules containing one CH_3SOH and one aromatic molecule/ion with cubic periodic boundary conditions in an isothermal–isobaric ensemble (NpT) at 298.15 K and 1.0 atm. Electrostatic interactions were computed using the particle-mesh Ewald method[33] with $\kappa = 0.33$ for charge screening and a 1.0-Å grid spacing with fourth-order splines for mesh interpolation. Real-space interactions (LJ and electrostatic) were cut off at 15 Å. A Nosé–Hoover thermostat[34] and an Andersen–Hoover barostat[35] maintained the temperature and pressure at the preset values with relaxation times of 0.1 and 0.2 ps, respectively. The equations of motion were integrated in 1-fs steps. All bonds involving H atoms were kept at their reference lengths using the RATTLE/Roll algorithm.[36]

Potential of mean force (PMF) calculations. CH_3SOH–aromatic binding free energies in bulk water were derived through umbrella sampling as described previously.[8,9,23,24] The value of r_{SX} (Fig. 2B) was sampled from 2.0 to 10.0 Å in 0.5-Å increments and a constant harmonic potential of force (10 kcal mol^{-1} Å^{-2}) was applied to bias the sampling. The system was simulated for 2.1 ns at each r_{SX} value and data acquired during the initial 0.1 ns were discarded. The unbiased PMF was reconstructed using the Weighted Histogram Analysis Method (WHAM).[37,38] A correction term, $2RT\ \ln(r_{SX})$ where R is the gas constant,[39] was added to the PMF to account for the radial variation in the entropy of the solute pairs.

Investigating the CH_3SOH–aromatics in bulk water

The bonding interactions and complexation geometry were investigated for each CH_3SOH–aromatic in bulk water using 100-ns MD simulations (200 000 frames) in 500 water molecules. O_{ar}–H/N_{ar}–H$\cdots$O/S and O–H$\cdots O_{ar}$/N_{ar} σ-type H-bonding (where the ar subscript indicates an aromatic N or O atom) between CH_3SOH and the aromatics was investigated using a cut-off of 2.5 Å for H$\cdots$O/N and 2.8 Å for H$\cdots$S H-bonds.[9,23,24,40] The r_{SX} values (Fig. 2B) were binned and the percentage of H-bonded structures plotted *vs.* r_{SX}[9,23,24] for the 200 000 structures analyzed for each complex. Contributions of π-type H-bonding (C–H/O–H$\cdots\pi_{ar}$) or O/S$\cdots\pi_{ar}$ interactions to complex stability in bulk water were evaluated from the $g_{ZX}(r)$ radial distribution functions representing the probability of finding any atom Z (H, C, O, S) of CH_3SOH at a distance r from the aromatic ring centroid X.

Geometries of the aqueous complexes were investigated by binning the θ_{SXY} angles at each r_{SX} (Fig. 2B). The number of structures in each bin $\rho(r_{SX}, \theta_{SXY})$ were counted and plots of the 2D PMF function,

$$\mathrm{PMF} = -RT \ln\left[\frac{\rho(r_{SX}, \theta_{SXY})}{2\pi r_{SX} \sin\theta_{SXY}}\right] \quad (3)$$

vs. $r_{SX}\sin\theta_{SXY}$ and $r_{SX}\cos\theta_{SXY}$ reveal the preference of the S atom for the face or the edge of the aromatic moiety, giving rise to en-face or edge-on geometry, respectively.[8,9,23,24]

Results

Geometry and electrostatic potential map of free CH_3SOH

Geometry optimization of CH_3SOH with MP2(full)/6-311++G(3df,3pd) yields a minimum energy structure with a dihedral angle $\phi_{CSOH} = 92.8^\circ$ and a dipole moment of 2.14 D. Conformers with $\phi_{CSOH} = 0^\circ$ and 180° are transition state (TS) structures lying 6.5 and 3.6 kcal mol^{-1}, respectively, above the most stable structure (Fig. 1A). MP2(full)/6-311++G(d,p) calculations predict $\phi_{CSOH} = 93.5^\circ$ and a dipole moment of 2.38 D for the stable structure of CH_3SOH and TS structures at 6.8 and 3.4 kcal mol^{-1} (Fig. 1A).

Examination of the electrostatic potential surface map calculated with MP2(full)/6-311++G(d,p) (Fig. 1B) sheds light on the reactivity of CH_3SOH. Its methyl and hydroxyl H atoms are characterised by maximum electropositive potentials ($V_{s,max}$) of 10–16.2 and 38.3 kcal mol^{-1}, respectively. Additionally, CH_3SOH possess a positive σ-hole (electron-deficient outer

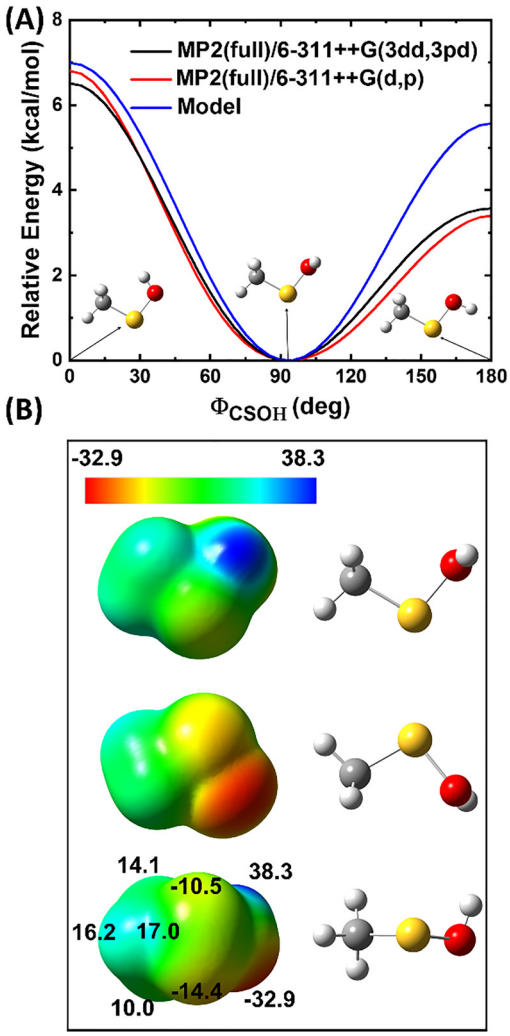

Fig. 1 Molecular properties of gaseous CH_3SOH. (A) Relative energy profile of CH_3SOH along the ϕ_{CSOH} torsional angle calculated with MP2(full)/6-311++G(3df,3pd) (black), MP2(full)/6-311++G(d,p) (red), and our additive model (blue). (B) Three orientations of the electrostatic potential map of the global minimum structure (ϕ_{CSOH} = 93.5°) calculated with MP2(full)/6-311++G(d,p) (left) and the corresponding dispositions of the atoms (right). The maps highlight the positive potential on the hydroxyl H (top), the negative potential on the hydroxyl O atom (middle) and the positive σ-hole extending from the S atom along the S–O bond (bottom). The numerical values of the potentials ($V_{s,max}$ or $V_{s,min}$, kcal mol^{-1}) on the atoms, lone pairs and the σ-hole are also given on the bottom surface.

lobes of a bonding p orbital)[23] with $V_{s,max}$ = 17 kcal mol^{-1} extending from the S atom along the S–O bond. Minimum electronegative potentials ($V_{s,min}$) are centred on the O (−32.9 kcal mol^{-1}) and S (−10.5 and −14.4 kcal mol^{-1}) atoms. Note that the S lone pairs are well separated in space[9,23,41] resulting in two distinct regions of $V_{s,min}$ whereas the overlapping electron density of the O lone pairs results in a single electronegative site on this atom.[15,42]

Our previous calculations on CH_3SH at the same level[9] revealed electrostatic potentials of 12.2, 15.3 and −18.4 kcal mol^{-1} on its methyl H, thiol H, and S atoms, respectively. Thus, Cys oxidation to CysSOH should generate a better H-bond donor and a better H-bond acceptor at the sulfenic O but not S atom.

Gas-phase geometries and interaction energies of the CH_3SOH–aromatics calculated with MP2(full)/6-311++G(d,p)

Fig. 2 shows the geometries of the global minimum energy gas-phase CH_3SOH complexes while Table 1 summarizes their key inter-fragment structural parameters (r_{SX} and θ_{SXY}, Fig. 2B) and interaction energies. Fig. S1–S7 and Tables S1–S7 of the SI present the corresponding properties of local-minimum conformers of the seven complexes. The large BSSE values observed in Table 1 and Tables S1–S7 are consistent with those we found previously for noncovalent interactions using the same level of

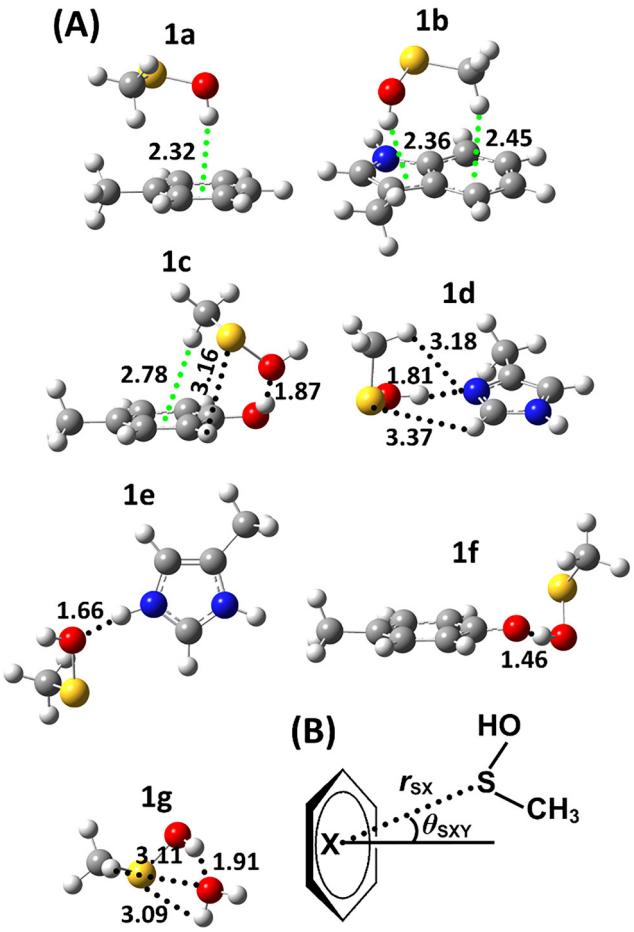

Fig. 2 (A) Optimized gas-phase geometry of the global minimum energy conformers of the CH_3SOH–aromatic and CH_3SOH–H_2O complexes. Structure of the (**1a**) toluene, (**1b**) 3-methylindole, (**1c**) 4-methylphenol (**1d**), 4-methylimidazole, (**1e**) 4-methylimidazolium, (**1f**) 4-methylphenolate and (**1g**) H_2O complex calculated with MP2(full)/6-311++G(d,p). The colour code for the atoms is H (white), C (grey), N (blue), O (red) and S (yellow). Inter-fragment σ- (black) and π-type (green) H-bonds are designated by the dotted lines. (B) Inter-fragment geometrical parameters of the CH_3SOH–aromatics where r_{SX} is the distance between the S atom and the aromatic ring centroid X (indole C_6 ring) and θ_{SXY} is the angle between atom S, X and any point Y on the vector normal to the ring plane that passes through X. The SI lists the atomic coordinates of all global and local minimum energy conformers.

Table 1 Properties of the global minimum conformers of the CH_3SOH–aromatic complexes in the gas phase[a]

Ligand (aa[b], complex)[a]	r_{SX}[a], Å	θ_{SXY}[a] degrees	E^c, kcal mol^{-1}	$E^{CP\,c}$, kcal mol^{-1}	$E^{MM\,d}$, kcal mol^{-1}	$E^{MM,opt\,d}$, kcal mol^{-1}	CH_3SOH charge[e]	IPV[f], eV	CH_3SOH spin density[g]
Toluene (Phe, **1a**)	3.93	27	−9.77	−4.85	−5.00	—	0.009	8.48 (8.45–8.98)	1.0
3-Methylindole (Trp, **1b**)	4.06	30	−13.05	−6.99	−6.40	—	−0.002	8.27 (7.65–8.90)	0.6
4-Methylphenol (Tyr, **1c**)	4.40	48	−12.41	−7.16	−5.95	—	0.024	8.60 (8.29–9.12)	0.0
4-Methylimidazole (His, **1d**)	4.45	87	−13.67	−10.26	−9.06	—	−0.038	8.02 (7.93–8.64)	1.0
4-Methylimidazolium ($HisH^+$, **1e**)	4.64	82	−21.40	−16.86	−8.75	−15.14	0.059	12.6 (11.9–12.8)	1.0
4-Methylphenolate (Tyr^-, **1f**)	5.09	83	−31.05	−25.86	−18.84	−24.70	−0.122	4.15 (3.66–4.21)	0.0
H_2O (**1g**)	3.27	—	−8.40	−5.87	−5.27	—	−0.013	8.64 (9.38)	1.0

[a] See structures of complexes in Fig. 2A; r_{SX} and θ_{SXY} are defined in Fig. 2B. The CH_3SOH–H_2O complex **1g** is included for reference and r_{SX} corresponds to the S–O(H_2O) distance. [b] Amino acid (aa) side chain modelled by the aromatic ligand. [c] BSSE-uncorrected (E) and corrected (E^{CP}) *ab initio* gas-phase interaction energies calculated with MP2(full)/6-311++G(d,p). [d] Interaction energies calculated with the default (E^{MM}) and optimized ($E^{MM,opt}$) force field (FF) where necessary. [e] Net charge (e) of CH_3SOH in the complex. [f] Vertical ionization potentials (IPV) from the *ab initio* calculations. The range of IPV values for the local minima conformers (SI Fig. S1–S7 and Tables S1–S7) is given in brackets. Calculated IPVs (eV) of the free ligands: CH_3SOH (9.20; this work), toluene (9.45),[9] 3-methylindole (7.88),[9] 4-methylphenol (8.77),[9] 4-methylimidazole (8.78),[9] 4-methylimidazolium (14.64),[24] 4-methylphenolate (3.31),[24] and H_2O (12.60).[9] [g] Spin density on CH_3SOH ligand following loss of one electron from the complex; a value of 1.0 indicates CH_3SOH oxidation and 0.0 aromatic oxidation.

theory.[9,23] Although no experimental data are available for the systems examined in this study, the BSSE-corrected (E^{CP}) interaction energies are expected to be reliable as demonstrated for other noncovalent complexes.[32] Based on their θ_{SXY} values, the complexes are assigned en-face/distorted en-face ($<30^\circ$), intermediate (30–60°) and edge-on ($>60^\circ$) geometries.

The optimized toluene complexes are characterized by O–H$\cdots\pi_{ar}$ (**1a**, S1g–S1i) or C–H$\cdots\pi_{ar}$ (S1a–S1f) π-type H-bonding, which accounts for their distorted en-face or borderline intermediate geometry (θ_{SXY} = 21–36°; Fig. 2, Table 1 and Fig. S1, Table S1). The significantly larger electropositive potential of the CH_3SOH hydroxyl *vs.* methyl H (Fig. 1B) explains the greater stability of **1a** and S1g–S1i (E^{CP} = −4.3 to −4.9 kcal mol^{-1}) *vs.* S1a–S1f (E^{CP} = −2.2 to −3.6 kcal mol^{-1}) (Table 1 and Table S1).

The 3-methylindole complexes are also stabilized by π-type H-bonding with distorted en-face or intermediate geometry (θ_{SXY} = 28–49°; Fig. 2, Table 1 and Fig. S2, Table S2). The larger electronegative potential of the indole C_6 ring *vs.* the phenyl ring[42] plus its simultaneous accommodation of two π-type H-bonds (**1b**) accounts for the greater stability of the methylindole *vs.* the toluene complexes (E^{CP} values, Table 1 and Table S1, S2). Furthermore, C–H$\cdots$O/S (**S2a**, **S2b**) and N_{ar}–H$\cdots$O **S2f**, **S2h**) σ-type H-bonds contribute to the stability of four of the ten optimized 3-methylindole complexes. Notably, the strong N_{ar}–H$\cdots$O σ-type H-bond present in both **S2f** and **S2h** shifts their θ_{SXY} values (47–49°, Table S2) towards the intermediate geometry (30–60°) midpoint.

Like the toluene and indole complexes, all 17 of the 4-methylphenol complexes are stabilized by π-type H-bonding (Fig. 2 and Fig. S3). Notably, 15 are additionally stabilized by σ-type H-bonds, resulting in distorted en-face and intermediate geometry (θ_{SXY} = 25–48°; Fig. 2 and Table 1, Fig. S3, Table S3). The two 4-methylphenol complexes **S3h** and **S3k** stabilized by π-type H-bonds only possess distorted en-face geometry (θ_{SXY} = 28 and 26°) and are essentially isoenergetic with toluene complex **1a**, reflecting the similar electrostatic surface of the phenol and benzene aromatic rings.[42] On the other hand, strong O_{ar}–H$\cdots$O σ-type H-bond explains the considerably higher stability and greater θ_{SXY} of **1c** and **3Sp** *vs.* **1a** (Table 1 and Table S3). Also, the 0.5–1.1 kcal mol^{-1} higher stability of **1c** and **S3p** relative to **S3m** and **S3o** with $O_{ar}\cdots$H–O σ-type H-bonding reveal that 4-methylphenol is a better H-bond donor than acceptor when interacting with CH_3SOH. Finally, the O_{ar}–H$\cdots$S σ-type H-bond stabilizes the intermediate geometry of **S3f**, **S3g**, **S3j**, **S3l** and **S3n** (Table S3).

CH_3SOH preferentially donates a H-bond to the pyridine-type N of 4-methylimidazole consistent with the electronegative potential of imidazole being centred over this atom.[42] Hence, the most stable 4-methylimidazole complexes (**1d**, **S4i**, **S4h**) exhibit edge-on geometry (θ_{SXY} = 71–87°; Table S4) due to strong O–H$\cdots N_{ar}$ σ-type H-bonding with the pyridine-type N (Fig. 1 and Fig. S4). The strength of this H-bonding is underscored by the significantly higher gas-phase affinity of CH_3SOH for 4-methylimidazole *vs.* the other neutral aromatics (E^{CP} values, Table 1). Conformers **S4f** and **S4g** also possess strong O–H$\cdots N_{ar}$ σ-type H-bonding but are additionally stabilized by π-type H-bonding, accounting for their intermediate geometry (θ_{SXY} = 41–42°; Table S4). In fact, seven (**S4a–S4g**) of the 10 optimized 4-methylimidazole complexes exhibit π-type H-bonding and the weakest (**S4a–S4c**) exhibit en-face geometry (θ_{SXY} = 6–22°; Table S4). These three complexes also exhibit weak σ-type C–H$\cdots N_{ar}$ H-bonding whereas stronger σ-type N_{ar}–H$\cdots$O H-bonding increases both the stability and θ_{SXY} (42–43°) of **S4d–S4e** (Table S4).

Imidazolium possesses an entirely electropositive surface ($V_{s,max}$ = 84 to 138 kcal mol^{-1}).[24] Hence, all but three (**S5b–S5d**) of the 14 optimized 4-methylimidazolium conformers are stabilized by strong σ-type H-bond donation from a ring N to the O or S atom of CH_3CSOH (N_{ar}–H$\cdots$O/S) (Fig. 1 and Fig. S5). **S5b–S5d** are also stabilized by strong C_{ar}–H$\cdots$O/S σ-type H-bond donation from the C atoms of 4-methylimidazolium. Given their σ-type H-bonding, all but one (**S5e**) of the cationic complexes exhibit edge-on geometry (θ_{SXY} = 61–90°; Table S5). **S5e** adopts intermediate geometry (θ_{SXY} = 35°; Table S5) since, in addition to σ-type N_{ar}–H$\cdots$S H-bonding, it is also stabilized by electrostatic attraction between the O lone pairs and the electropositive surface of the imidazolium ring. Finally, we note that **1e** with a single N_{ar}–H$\cdots$O σ-type H-bond is ∼8 kcal mol^{-1}

more stable than **S5a** with a single N_{ar}–H···S σ-type H-bond (Table S5 and Fig. 1, Fig. S5) due to the considerably larger $V_{s,min}$ at the O *vs.* S atom of CH_3SOH (Fig. 1B).

Phenolate possesses an entirely electronegative surface ($V_{s,min}$ = −60 to −131 kcal mol^{-1}).[24] The global minimum CH_3SOH–4-methylphenolate complex **1f**, the most stable by far of the gas-phase CH_3SOH complexes (E^{cp} ∼ −26 kcal mol^{-1}; Table 1), possesses a single very strong O–H···O_{ar} σ-type H-bond and exhibits edge-on geometry (Fig. 2A). In contrast, the five local minimum phenolate conformers all possess π-type C/O–H···π_{ar} H-bonding and four **S6a–S6d** adopt en-face geometry (θ_{SXY} = 15–29°; Fig. S6 and Table S6). Also, the high stability of **S6b**, **S6c** (E^{cp} ∼ −13 kcal mol^{-1}; Table S6) with just C/O–H···π_{ar} H-bonding (Fig. S6) underscores the strength of π-type H-bonding with the phenolate ring.

Two stable structures were optimized for the CH_3SOH–H_2O complex with CH_3SOH acting as a H-bond donor (**1g**, E^{CP} = −5.87 kcal mol^{-1}) or acceptor (**S7a**, E^{CP} = −4.94 kcal mol^{-1}). The ∼1 kcal mol^{-1} higher stability of **1g** indicates that CH_3SOH is a slightly better H-bond donor than H_2O.

Benchmarking the MP2(full)/6-311++G(d,p) calculations

Before examining the redox properties of the complexes, we evaluated the performance of the MP2(full)/6-311++G(d,p) calculations by comparing the E^{CP} interaction energies of the global minimum conformers (Table 1) against those obtained using DFT (B3LYP, M062X) or CCSD(T) methods, combined with the same [6-311++G(d,p)] or larger basis sets [6-311++G(3df,3pd) and aug-cc-pVQZ]. Due to its failure to account for dispersion interactions,[43] B3LYP underestimates the stability of **1a–c**, which are largely stabilized by dispersive π-type[44] *vs.* coulombic σ-type H-bonding in complexes **1d–g** (Fig. 2A). Results using the M062X, MP2(full) and CCSD(T) functionals are closer (Fig. 3), in particular the E^{CP} values calculated with MP2(full)/6-311++G(d,p) fall within an average unsigned deviation of only 1 kcal mol^{-1} from those obtained using CCSD(T)/6-311++G(d,p), the most computationally expensive model chemistry examined here. Thus, we conclude that MP2(full)/6-311++G(d,p) is an excellent compromise between accuracy and computational cost in modelling the CH_3SOH–aromatics, which justifies its use in this study. In addition, the MP2(full)/6-311++G(d,p) method is chosen here as it was shown to yield interaction energies in good agreement with experiment for other noncovalent interactions[32] and to allow direct comparison with the sulfur–aromatic interactions we investigated previously using this method.[8,9]

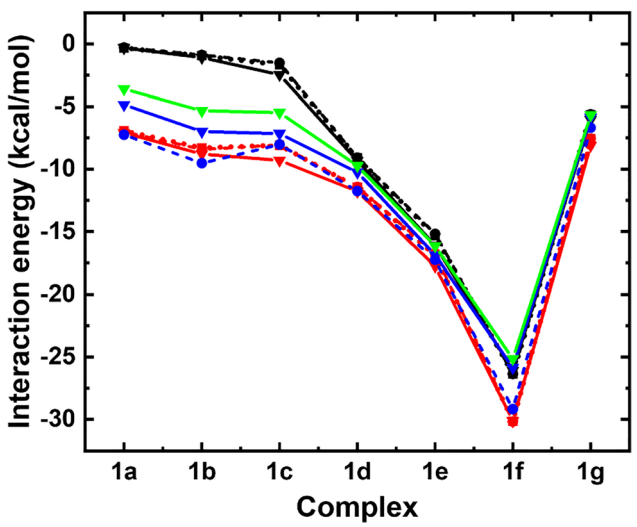

Fig. 3 Benchmarking the MP2(full)/6-311++G(d,p) calculations (solid blue line) for the global minimum conformers of the CH_3SOH–aromatic and CH_3SOH–H_2O complexes. The BSSE-corrected interaction energies E^{CP} of the global minimum conformers (Fig. 2A) calculated with the B3LYP (black), M062X (red), MP2(full) (blue) and CCSD(T) (green) functionals using the 6-311++G(d,p) (triangles, solid lines), 6-311++G(3df,3pd) (circles, dashed lines) and aug-cc-pVQZ (squares, dotted lines) basis sets. Note that the B3LYP (black) and M062X (red) functionals yield E^{CP} values that are essentially basis-set independent. Also, due to their high computational cost, we did not perform MP2(full)/aug-cc-pVQZ, CCSD(T)/6-311++G(3df,3pd) or CCSD(T)/aug-cc-pVQZ calculations.

Redox properties of the gas-phase CH_3SOH–aromatics

To predict the impact of complexation on the redox behaviour of CH_3SOH, we calculated at the MP2(full)/6-311++G(d,p) level the IPV of the 69 stable complexes found here plus the charge on the CH_3SOH ligand and its spin density following loss of an electron from each complex (Table 1 and Tables S1–S7). As we noted previously,[9,23,24] the ligand with the smaller IPV gets oxidized when the free ligands exhibit considerably different IPVs (footnote *f*, Table 1). Thus, CH_3SOH (9.20 eV) is the centre oxidized in all the 4-methylimidazolium (14.64 eV) complexes (Table S5) while the phenolate (3.31 eV) is oxidized in all the 4-methylphenolates (Table S6). Strong σ-type H-bonding promotes transfer of ∼0.1*e* from CH_3SOH to 4-methylimidazolium (Table S5) and from 4-methylphenolate to CH_3SOH in the most stable complexes (Table S6). Consequently, the IPVs of imidazolium complexes are up to 3.6 eV higher than that of free CH_3SOH (Table S5) and the IPVs of the phenolates are up to 0.9 eV higher than that of free 4-methylphenolate (Table S6).

In the toluene complexes, π-type H-bond donation to the ring results in charge transfer to CH_3SOH (Fig. 1 and Fig. S1). However, the small positive charge on CH_3SOH in all the toluene complexes except **S1c** (Table S1) suggests that weak long-range S–aromatic interactions counteract charge transfer from the ring. Nonetheless, CH_3SOH is the center oxidized and the IPVs of the complexes lie ≤0.75 eV below that of free CH_3SOH (Table S1). CH_3SOH also acts as an H-bond donor and is the center oxidized in most of the 4-methylimidazole complexes (Table S4). Strong σ-type O–H···N_{ar} H-bonding promotes the transfer of up to 0.04 e to CH_3SOH and the IPVs of the complexes are up to 1.3 eV lower than that of free CH_3SOH (Table S4).

CH_3SOH is oxidized in only four of its ten 3-methylindole complexes, including its most stable complexes, **1b** and **S2i** (Table S2) with exclusively π-type O–H···π_{ar} H-bonding. In contrast, CH_3SOH is oxidized in 11 of its 17 complexes with 4-methylphenol but not in **1c** and **S3p**, the two most stable

complexes (Table S3). Transfer $\sim$0.02e to the aromatic *via* strong σ-type O_{ar}–H$\cdots$O H-bond donation precipitates ring donation in **1c** and **S3p** (Table S3). The centre oxidized switches to CH_3SOH in **S3o** and **S3m** (Table S3) with σ-type O–H$\cdots O_{ar}$ H-bonding (Fig. 1 and Fig. S3). Since **S3o** and **S3m** are slightly less stable than **1c** and **S3p** (E^{CP}, Table S3), the O atom of CH_3SOH is a slightly better H-bond acceptor than that of 4-methylphenol.

Free CH_3SOH (9.20 eV) has significantly smaller IPV than H_2O (12.60 eV) so CH_3SOH is the centre oxidized in the two H_2O complexes, **1g** and **S7a** (Table S7). Nonetheless, these complexes exhibit IPVs $\sim$0.6 eV lower (**1g**) and $\sim$0.2 eV higher (**S7a**) than free CH_3SOH (Table S7) since H_2O is a H-bond acceptor in the former and donor in the latter (Fig. 1 and Fig. S7).

Optimized force field (FF) for CH_3SOH and its interaction with the aromatic ions

To perform MD simulations in bulk water, a new potential model was optimized for CH_3SOH and calibrated for its interactions with the aromatic ions. The optimized FF is reported in the SI. Our additive model yields an equilibrium geometry for CH_3SOH characterized by ϕ_{CSOH} = 93.2° and a dipole moment of 2.11 D, in good agreement with the MP2(full)/6-311++G-(3df,3pf) values (92.8° and 2.14 D). The model also finds TS conformers with ϕ_{CSOH} = 0° and 180° at 7.0 and 5.6 kcal mol^{-1} above the ground state *vs.* 6.5 and 3.6 kcal mol^{-1} for the *ab initio* values (Fig. 1A). The model also reproduces the shape of the ϕ_{CSOH} potential energy surface within $\sim$2 kcal mol^{-1} over the minimum energy region (ϕ_{CSOH} = 60–130°, Fig. 1A), thereby capturing the equilibrium geometry while still allowing the conformational flexibility relevant to ambient fluctuations.

The default FF interaction energies (E^{MM}) underestimate E^{CP} of the CH_3SOH–4-methylimidazolium and CH_3SOH–4-methylphenolate complexes by an average of 5.4 and 3.2 kcal mol^{-1}, respectively. In comparison, E^{MM} for the neutral aromatic and H_2O complexes deviate from E^{CP} by an average unsigned error of only 0.7 kcal mol^{-1} (Table 1 and Tables S1–S7). Optimization of the O–N and O–O pair-specific LJ parameters allows calibration of the model *vs.* the *ab initio* PECs (Fig. 4) to give $E^{MM,opt}$ that deviate from E^{CP} by average unsigned errors of 1.9 and 1.1 kcal mol^{-1} (Tables S5 and S6). Hence, adoption of the optimized pair-specific LJ parameters ($\epsilon_{ON} = -2.200$ kcal mol^{-1}, $R_{min,ON}$ = 2.865 Å for 4-methylimidazolium; $\epsilon_{OO} = -0.700$ kcal mol^{-1}, $R_{min,OO}$ = 2.750 Å for 4-methylphenolate) ensures that interactions of CH_3SOH with the charged aromatics are adequately described.

Stability and bonding of the CH_3SOH–aromatics in bulk water

The affinity of CH_3SOH for the aromatics was investigated in bulk water using PMF calculations (Fig. 5 and Table 2). Solute–solute interactions are usually weaker in bulk water *vs.* the gas phase due to competition from H_2O–solute interactions.[8,9,23,24,27–32] The CH_3SOH complexes of the neutral aromatics display binding free energy minima in bulk water (~ -0.6 kcal mol^{-1}; Table 2) 7–20-fold less than those in the gas phase (E^{CP} values; Table 1).

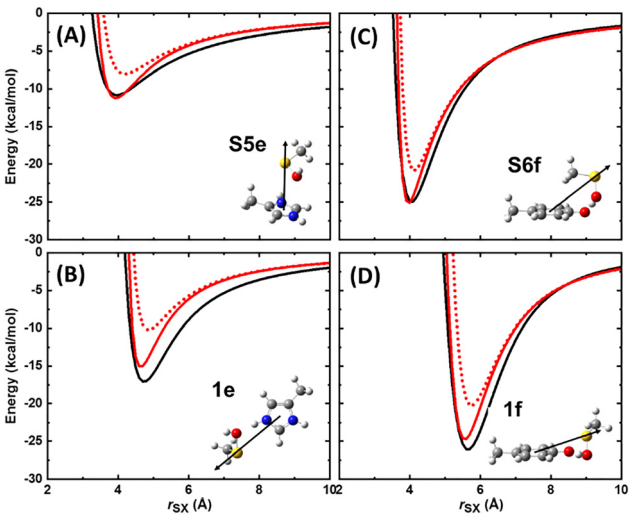

Fig. 4 Potential energy curves for selected CH_3SOH complexes of 4-methylimidazolim (A and B) and 4-methylphenolate (C and D) from *ab initio* calculations with MP2(full)/6-311++G(d,p) (solid black lines), the default FF model (dotted red lines), and the optimized model (solid red lines). PEC were calculated by scanning the selected intermolecular coordinate r_{SX} (Fig. 2B) shown for each structure as detailed under Computational methods.

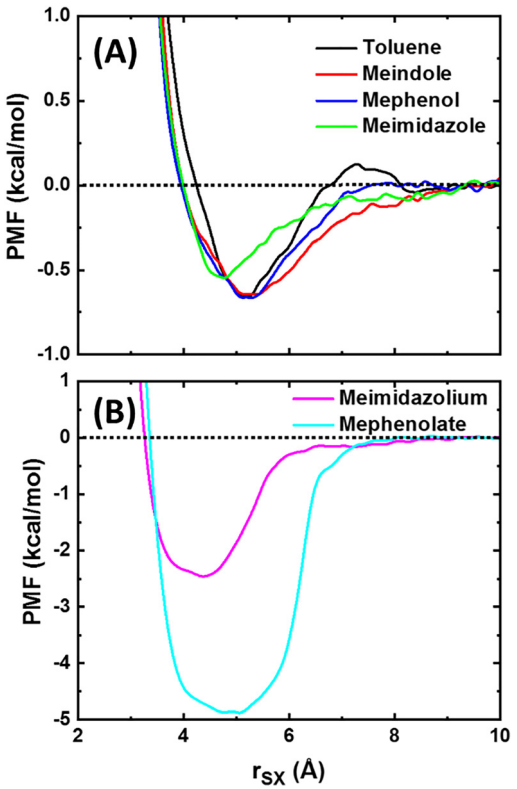

Fig. 5 Potentials of mean force (PMFs) between the S atom of CH_3SOH and the ring centroid of (A) toluene (black), 3-methylindole (red), 4-methylphenol (blue), 4-methylimidazole (green); and (B) 4-methylimidaolium (pink), and 4-methylphenolate (cyan). The pair-specific LJ parameters optimized in this work for CH_3SOH interaction with the aromatic ions and those optimized previously for H_2O–phenolate interaction[8] were used to derive the PMFs for the aromatic ion complexes.

Table 2 Values of r_{sx} (Å) and PMF minima (kcal mol^{-1}) in bulk water for the CH_3SOH–aromatics[a]

Aromatic	r_{SX}	PMF
Toluene	5.3	−0.65
3-Methylindole	5.3	−0.65
4-Methylphenol	5.3	−0.65
4-Methylimidazole	4.8	−0.55
4-Methylimidazolium	4.8	−2.5
4-Methylphenolate	5.0	−4.9

[a] Data from Fig. 5.

However, ionization of the aromatic greatly increases its affinity for CH_3SOH in bulk water (Fig. 5) such that CH_3SOH has only ∼5-fold less affinity for the aqueous *vs.* gaseous charged aromatics (Tables 1 and 2).

To characterize bonding in the aqueous complexes, we next examine the probability of finding atom Z (H, C, O or S) of CH_3SOH at a distance r_{ZX} from the aromatic ring centroid X (Fig. 2B; C_6 ring of indole). This probability is determined from the 100-ns MD simulations and expressed as radial distribution function, $g_{ZX}(r)$. Notably, $g_{HX}(r)$ displays a peak centred at ∼5.0 Å for the toluene, 3-methyindole and 4-methylphenol complexes but at ∼4.3 Å for complexes of the smaller 4-methylimidazole ring (Fig. 6A–D). Also, the high electrostatic potentials at the hydroxyl atoms (Fig. 1B) results in higher intensities of the hydroxyl $g_{HX}(r)$ peak centred at r_{HX} = 2.3 Å and the $g_{OX}(r)$ shoulder at r_{OX} = 3.2 Å *vs.* the methyl $g_{HX}(r)$ peak and $g_{CX}(r)$ shoulder at r_{HX} = 2.3 Å and r_{CX} < 3.5 Å, respectively (Fig. 6A–D). Finally, we note that $g_{SX}(r)$ is less intense than $g_{CX}(r)$ or $g_{OX}(r)$ at r_{ZX} < 4.0 Å (Fig. 6A–D), mirroring the lower frequency of S···π_{ar} *vs.* C–H···π_{ar} or O–H···π_{ar} interactions in the gas-phase (Fig. S1–S6).

Based on the MD simulations, ∼10–17% of the 4-methylimidazole complexes are stabilized by O–H···N_{ar} σ-type H-bonding at r_{SX} = 3.2–4.1 Å (Fig. 7A). N–H_{ar}···O bonding is present in ∼2% of these complexes (Fig. 7A), confirming that CH_3SOH is a better H-bond donor than acceptor in its 4-methylimidazole complexes as seen in the gas phase (Fig. 2A and Fig. S4). In the 4-methylphenol complexes, both O–H···O_{ar} and O–H_{ar}···O σ-type H-bonding is ≲2% as is N–H_{ar}···O σ-type H-bonding in 3-methylindole (Fig. 7A). Note that N/O–H_{ar}···S σ-type H-bonded structures are <2% and their percentages are not plotted in Fig. 7A.

Intense $g_{OX}(r)$ peaks at r_{OX} = 3.0 and 3.8 Å plus the hydroxyl $g_{HX}(r)$ peak at r_{HX} = 3.3 Å signal strong N_{ar}–H···O H-bonding in CH_3SOH–4-methylimidazolim (Fig. 6E). Likewise, the sharp $g_{SX}(r)$ peak at r_{SX} = 4.4 Å suggests a sizable contribution from N_{ar}–H···S σ-type H-bonding whereas the weak $g_{CX}(r)$ peaks at r_{CX} = 4.5 and 5.3 Å combined with negligible methyl $g_{HX}(r)$ intensity are consistent with repulsive interactions between the aromatic cation and the electropositive methyl H atoms (Fig. 6E). The CH_3SOH–4-methylphenolate complex (Fig. 6F) exhibits dominant hydroxyl $g_{HX}(r)$ peaks at r_{HX} = 2.1 and 3.5 Å plus $g_{OX}(r)$ peaks at r_{OX} = 3.1 and 4.3 Å. These peaks signal strong O–H···π_{ar} and O–H···O_{ar} H-bonding whereas the baseline intensity of $g_{HX}(r)$ indicates negligible C–H···O_{ar} H-bonding.

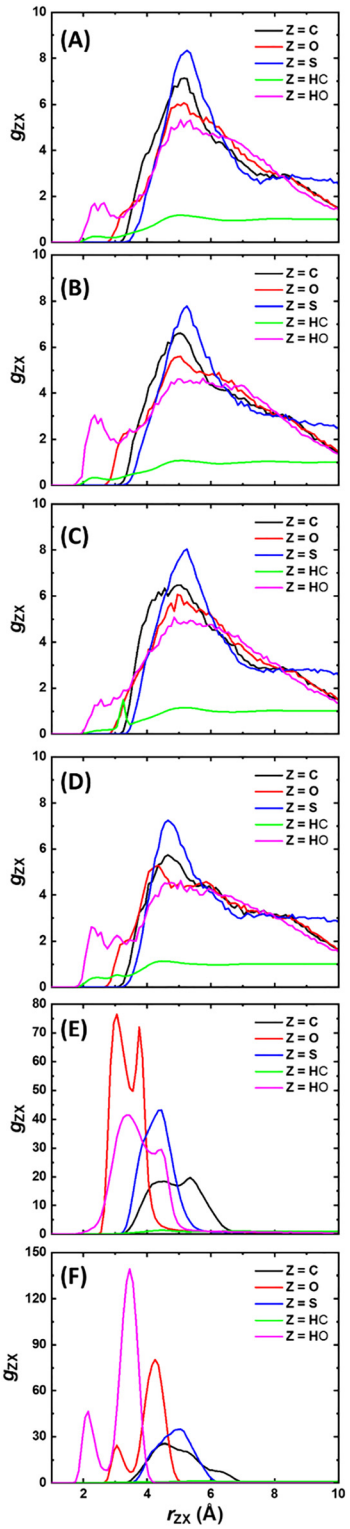

Fig. 6 Radial distribution of CH_3SOH atoms around the aromatic ring centroid in bulk water. C–X (black), O–X (red), S–X (blue), CH_3–X (green) and OH–X (pink) radial distribution function $g_{ZX}(r)$ *vs.* Z–X distance where Z is C, O, S or H atom of CH_3SOH and X is ring centroid of: (A) toluene, (B) 3-methylindole, (C) 4-methylphenol, (D) 4-methylimidazole C_6 ring, (E) 4-methylimidazolium and (F) 4-methylphenolate in bulk water at 298.15 K. Plots constructed from 100-ns MD simulations of the complexes.

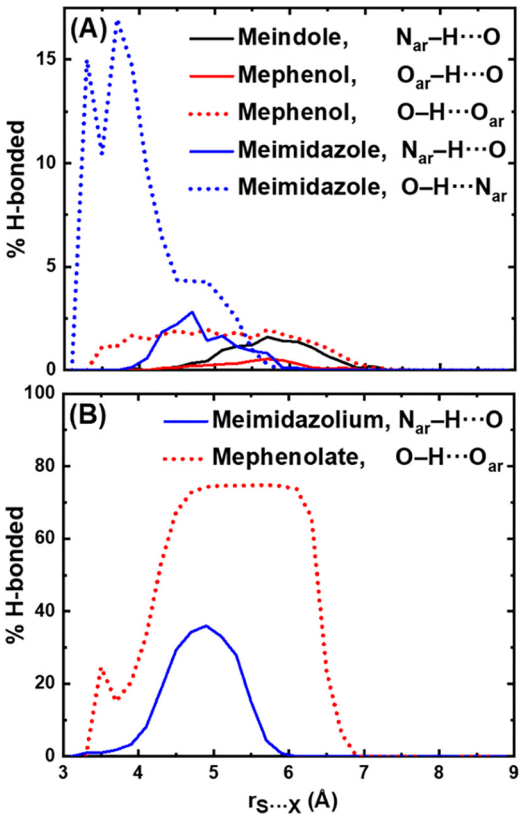

Fig. 7 Percentages of N/O–H_{ar}···O (solid lines) and O–H···N_{ar}/O_{ar} (dotted lines) σ-type H-bonded structures in the (A) neutral and (B) charged CH_3SOH–aromatics in bulk water at 298.15 K as a function of r_{SX}, the distance between the S atom of CH_3SOH and the ring centroid X (C_6 ring of indole; see Fig. 2B). Plots were constructed from the 100-ns MD simulations of the complexes and the H-bonded and aromatic (ar subscript) atoms are indicated in the panels. Less than 2% of the complexes possess N/O–H_{ar}···S σ-type H-bonds so their percentages are not plotted.

Again, mirroring the gas phase, σ-type H-bonding is dominant in the charged aqueous CH_3SOH complexes (Fig. 7B). Approximately 35% of the 4-methylimidazolium complexes are stabilized by N–H_{ar}···O H-bonding at r_{SX} = 4.8 Å while 25% and 75% of the 4-methylphenolate complexes are stabilized by O–H···O_{ar} H-bonding at r_{SX} = 3.5 and 4.7–6.1 Å, respectively, (Fig. 7B). Thus, the greater percentage of σ-type H-bonding in the anionic complexes explains their greater stability *vs.* the cationic complexes (Fig. 5B).

Geometry of the CH_3SOH–aromatics in bulk water

The stabilities of the aqueous complexes *vs.* geometry are plotted in Fig. 8.[8,9,23,24] The 2D plots of the PMF dependence on θ_{SXY} and r_{SX} (Fig. 2B) reveal that the most stable neutral and cationic complexes are characterized by en-face binding ($\theta_{SXY} < 30°$; Fig. 8A–E) whereas stable anionic 4-methylphenolate complexes adopt both en-face and intermediate geometry (θ_{SXY} = 10–60°; Fig. 8F). The relative stability of the latter over a wide range of θ_{SXY} values (Fig. 8F) is likely a consequence of H-bonding over an also wide range of r_{SX} (Fig. 7B).

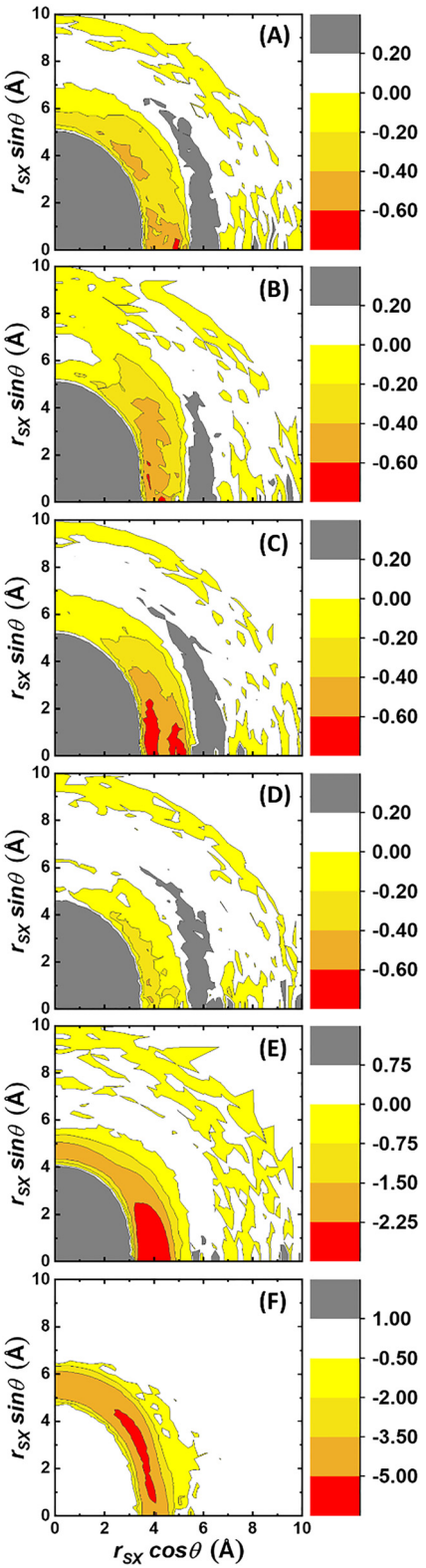

Fig. 8 Variation in stability of the aqueous CH_3SOH–aromatics with geometry. The 2D heat maps show the potential of mean force (PMF, kcal mol^{-1}) for the CH_3SOH complex of (A) toluene, (B) 3-methylindole, (C) 4-methylphenol, (D) 4-methylimidazole, (E) 4-methylimidazolium, and (F) 4-methylphenolate from the 100-ns MD simulations in bulk water at 298.15 K. The PMF is given by eqn (3); r_{SX} and θ_{SXY} are defined in Fig. 2B. The PMF value for idealized en-face geometry θ_{SXY} = 0°) falls on the *x*-axis and that for edge-on geometry (θ_{SXY} = 90°) falls on the *y*-axis.

Discussion

In the present study, we have characterized both the gas-phase and aqueous complexes of CH_3SOH, a model of CysOH, with toluene, 3-methylindole, 4-methylphenol, 4-methylphenolate, 4-methylimidazole, and 4-methylimidazolium, models of Phe, Trp, the neutral and charged side chains of Tyr and His, and with H_2O. We identified a total of 69 stable gas-phase structures and investigated their interaction energies with MP2(full)/6-311++G(d,p). The global minimum-energy conformers display interaction energies in the range −4.9 to −25.9 kcal mol^{-1} (Table 1). Using the new additive FF model developed for CH_3SOH and the CHARMM36 FF for the aromatics, the stability of the CH_3SOH–aromatic complexes in water was measured. The model predicts maximum binding free energies of −0.55 to −0.65 for the neutral aqueous complexes, and values of −2.5 and −4.9 kcal mol^{-1} for the cationic and anionic complexes, respectively (Table 2). We previously reported that imidazolium possesses an entirely electropositive ($V_{s,max}$ = +84 to +138 kcal mol^{-1}) surface and phenolate an entirely electronegative surface ($V_{s,mjn}$ = −60 to −131 kcal mol^{-1}) surface.[24] Thus, these ligands form strong ion–dipole and H-bonding interactions, as reflected here in higher stabilities for the charged CH_3SOH *vs.* neutral aqueous complexes (Tables S1–S6).

Nature of H-bonding controls the geometry of the complexes

CH_3SOH binds toluene strictly by π-type H-bonding (O/C–H···π_{ar}) leading to distorted en-face or borderline intermediate geometry for the optimized CH_3SOH–toluene structures (θ_{SXY} = 21°–36°; Fig. 2, Table 1 and Fig. S1, Table S1). Both π- and σ-type H-bonding is present in the 3-methylindole and 4-methylphenol complexes, which consequently adopt highly distorted en-face or intermediate geometry (θ_{SXY} = 28°–49°; Fig. 2, Table 1 and Fig. S2, S3, Tables S2, S3). Likewise, σ-type H-bonding is responsible for edge-on CH_3SOH binding to 4-methylimidazole and 4-methylphenolate (O–H···N_{ar}/O), which additionally exhibit π-type H-bonding and a broad range of θ_{SXY} values (6°–87°; Fig. 2 and Fig. S4, S6, Tables S4, S6). CH_3SOH binds 4-methylimidazolium strictly edge-on (θ_{SXY} = 60°–90°) *via* σ-type H-bonding (N–H_{ar}···O/S) with the sole exception of **S5e** (θ_{SXY} = 35°), which is stabilized by electrostatic attraction between the O and S lone pairs and the electron-deficient surface of the imidazolium ring (Fig. 1 and Fig. S5).

Nature of H-bonding controls the redox properties of the complexes

Computational[9,23,24] and experimental[45–48] investigations reveal that noncovalent interactions can significantly alter the redox properties of interacting fragments. Both the difference in IPV of the fee ligands and the geometry of the complex determine the centre oxidized. Notably, H-bond donation renders the donor more electron-rich and the acceptor more electron poor. Thus, in complexes between fragments of similar IPV, the fragment that H-bond donates often gets oxidized, especially if the H-bond is strong (Fig. S1–S4).[9,23,24]

Focusing just on the five most stable complexes for each of the four neutral aromatics reveals that CH_3SOH functions as a H-bond donor 15 out of 20 times and is the centre oxidized (Tables S1–S4). Furthermore, the IPV values of the most stable complexes are ∼1 eV lower than that of free CH_3SOH indicating that strong H-aromatic interactions render CH_3SOH more oxidizable. The aromatic is oxidized in the 4-methylphenol (Tyr) and 3-methylindole (Trp) complexes where the phenol O (**1c**, **S3p**) and indole N (**S2h**, **S2f**) act as H-bond donors (Tables S2 and S3). Presumably, H-bond donation by CH_3SOH is insufficient to depress its IPV and become the centre oxidized in **S2g**. In fact, weaker CH_3SOH H-bond donation in **S2g** *vs.* **S2i** is reflected in the relative lengths of the π-type O–H···π_a H-bonds in these complexes (2.41 *vs.* 2.30 Å; Fig. S2).

Free 4-methylimidazolium (14.64 eV)[24] and 4-methylphenolate (3.31 eV)[24] have IPV values much greater and smaller, respectively, than free CH_3SOH (9.20 eV, Table 1). Hence, the sulfenic acid is the centre oxidized in all complexes of the former and the aromatic in all complexes of the latter (Tables S5 and S6).

Affinity of CH_3SOH *vs.* CH_3SH for the aromatics

We previously reported E^{CP} values (kcal mol^{-1}) at the MP2(full)/6-311++G(d,p) level for the gas-phase CH_3SH complexes,[8,9] and Table 3 shows that their global minimum conformers are 1.4–2.7-fold weaker than the CH_3SOH analogues. This arises because the electrostatic potentials ($V_{s,max}$, $V_{s,min}$; kcal mol^{-1}) on the H (15.3) and S (−18.4) atoms of CH_3SH[15] are considerably smaller than those of the H (38.3) and O (−32.9) atoms of CH_3SOH (Fig. 1B), rendering the latter a stronger H-bond donor and acceptor.

Table 3 Properties of the global minimum energy conformers of the CH_3SOH– *vs.* CH_3SH–aromatics in the gas phase and bulk water (aq)

	CH_3SOH–aromatic					CH_3SH–aromatic				
Aromatic (complex)[a]	r_{SX}, Å[a]	E^{CP} [a], kcal mol^{-1}	r_{SX} [b] (aq), Å	PMF (aq)[b], kcal mol^{-1}	IPV[a], eV	r_{SX}, Å	E^{CP} kcal mol^{-1}	r_{SX} (aq)[d], Å	PMF (aq)[d], kcal mol^{-1}	IPV, eV
Toluene (**1a**)	3.93	−4.85	5.3	−0.65	8.48	3.66[c]	−3.14[c]	5.0[d]	−0.7[d]	8.69[e]
3-Methylindole (**1b**)	4.06	−6.99	5.3	−0.65	8.27	4.01[c]	−5.04[c]	5.1[d]	−0.6[d]	9.02[e]
4-Methylphenol (**1c**)	4.40	−7.16	5.3	−0.65	8.60	4.11[c]	−5.12[c]	5.0[d]	−1.0[d]	8.81[e]
4-Methylimidazole (**1d**)	4.45	−10.26	4.8	−0.55	8.02	4.42[c]	−3.80[c]	4.4[d]	−0.9[d]	8.64[e]
4-Methylimidazolium (**1e**)	4.64	−16.86	4.8	−2.50	12.6	4.37[f]	−11.44[f]	4.0[h]	−4.7[h]	13.26[i]
4-Methylphenolate (**1f**)	5.09	−25.86	5.0	−4.90	4.15	4.41[g]	−12.84[g]	3.5[h]	−3.2[h]	4.58[i]

[a] From Table 1 this work. [b] From Table 2 this work. [c] From Table 5 of ref. 9. [d] From Table 7 of ref. 9 (note average r_{SX} values given here). [e] From Table 6 of ref. 9. [f] From Table S3 of ref. 8. [g] From Table S7 of ref. 8. [h] From Fig. S8 this work. [i] Calculated with MP2(full)/6-311++G(d,p) this work.

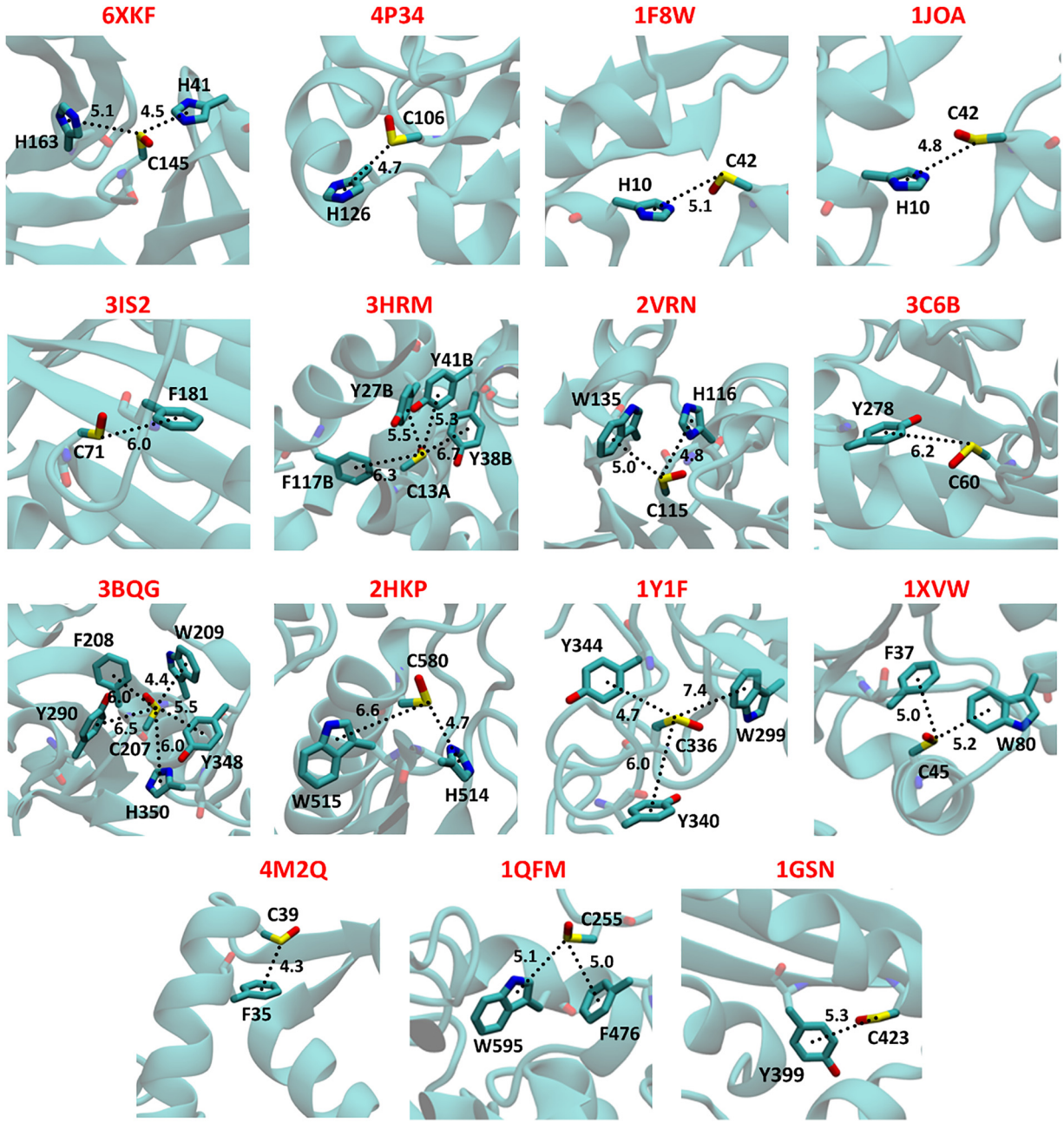

Fig. 9 CysOH–aromatic interactions retrieved from the Protein Data Bank. PDB protein IDs are labelled in red and their backbones represented as ribbons. The CysOH (C) and aromatic residues within 5 Å are represented as sticks with CPK atom colouring. The dotted lines indicate the r_{sx} values (Å) defined in Fig. 2B. The 15 structures presented here were retrieved from the PDB as outlined in section "CysOH–aromatic motifs in proteins" of the Discussion.

CH_3SH (9.17 eV)[9] and CH_3SOH (9.20 eV, Table 1) possess similar IPVs, explaining why Cys to CysOH oxidation is reversible. Table 3 reveals that the IPVs of the CH_3SOH–aromatics are 0.2 to 0.75 eV lower than those of the CH_3SH–aromatics, which should attenuate spontaneous reduction of the sulfenic acid back to the thiol and thereby serve to stabilize the former.

Before comparing the aqueous aromatic complexes, it is salient to compare their H_2O complexes. Two stable structur were optimized here for the CH_3SOH–H_2O complex (Table S7) with CH_3SOH as a H-bond donor (**1g**, E^{CP} = −5.87 kcal mol^{-1}) and acceptor (**S7a**, E^{CP} = −4.94 kcal mol^{-1}). CH_3SOH is a better H-bond donor than H_2O since **1g** is ∼1 kcal mol^{-1} more stable than **S7a**, whereas H_2O is a better H-bond donor than CH_3SH. Furthermore, the global minimum conformer of CH_3SH–H_2O with S as an H-bond acceptor (E^{CP} = −3.01 kcal mol^{-1})[8] is ∼2 kcal mol^{-1} less stable than **S7a**, reflecting the magnitude of $V_{s,min}$ (kcal mol^{-1}) on the thiol S (−18.4)[15] and the sulfenic O (−32.9; Fig. 1b).

Strong H-bonding between CH_3SOH and H_2O leads to ∼0–40% lower PMFs for the aqueous CH_3SOH–aromatics *vs.* their

CH_3SH analogues (Table 3).[8,9] However, 4-methylphenolate is a better H-bond acceptor than H_2O so its CH_3SOH complex is ~1.5-fold more stable than its CH_3SH complex (Table 3) due to the greater strength of O–H···O_{ar} *vs.* S–H···O_{ar} H-bonding. Finally, we note that the CH_3SH–aromatics,[8,9,23,24] like the CH_3SOH–aromatics (Fig. 8), favour en-face and intermediate association in water.

CysOH–aromatic motifs in proteins

To examine cysteine sulfenic acid–aromatic interactions in proteins, the Protein Data Bank (PDB) was queried on 15 June 2025 using the keyword ''sulfenic'' as a search term. This search retrieved 86 protein structures with 29 nonredundant structures containing a CysOH. The remaining 57 structures were either redundant or included a ligand with a sulfenic acid group. Markedly, in 15 of the 29 nonredundant structures an aromatic ring is within 5 Å of the CysOH side chain (Fig. 9). A recent survey[49] of Cys oxidation in proteins revealed that the probability of finding His close to non-oxidized Cys corresponds to the average prevalence of His in proteins but jumps ~3-fold around CysOH. His can act as proton acceptor from Cys,[9] lowering its pK_a and rendering the thiol more oxidizable.[49] Earlier protein profiling also identified His as a key residue in the modification of Cys to CysOH.[50] Furthermore, strong σ-type H-bonding would significantly stabilize the nascent CysOH–His relative to Cys–His (Table 3), making the latter more prone to oxidation, while stabilizing CysOH, which is susceptible to further reaction.[2] We note the presence of His near CysOH in 7 of the 15 structures in Fig. 9 with r_{sx} values of 4.5–5.1 Å close to those of **1d** and **1e** in 6 of these 7 structures (Table 3). Additionally, a Tyr with a r_{sx} value of 4.7–5.5 Å similar to those of **1c** and **1f** (Table 3) is found in 5 structures in Fig. 9, again signalling possible strong σ-type H-bonding.

The literature survey[49] also revealed a ~2-fold greater probability of finding crystallographic H_2O in the proximity of CysOH than Cys. This is consistent with stronger H-bonding of CH_3SOH *vs.* CH_3SH to H_2O, which accounts for the relative stability of their complexes in bulk water (Table 3) as discussed in the previous section. However, deprotonation of a neighbouring Tyr or protonation of a neighbouring His in a solvent-exposed protein region may favour and supress CysOH formation, respectively, based on the data for the ionized aromatics in bulk water in Table 3).

Given that reversible oxidation of Cys to CysOH is key in regulating function, catalysis and signalling of many proteins,[2] control of the redox activity of protein-based Cys residues by their protein microenvironment is of vital importance in biology. Therefore, an in-depth survey of S–aromatic interactions in the PDB is warranted considering the data summarized in Table 3 but outside the scope of the current work.

Conflicts of interest

There are no conflicts to declare.

Data availability

All data are presented in the main text and the SI. Supplementary information: 7 figures showing the optimized geometry of local minima conformers of all complexes, 7 tables showing the structural and energetic properties of these conformers, atomic coordinates of all (local + global) optimized geometries, force field parameters for CH_3SOH, and the PMFs calculated for MeSH-aromatic ions complexes in water. See DOI: **https://doi.org/10.1039/d5cp02976g**.

Acknowledgements

This work was supported by a research grant from the Natural Sciences and Engineering Research Council (NSERC) of Canada awarded to AME.

References

1 A. Miseta and P. Csutora, Relationship Between the Occurrence of Cysteine in Proteins and the Complexity of Organisms, *Mol. Biol. Evol.*, 2000, **17**(8), 1232–1239, DOI: **10.1093/oxfordjournals.molbev.a026406**.
2 L. J. Alcock, M. V. Perkins and J. M. Chalker, Chemical methods for mapping cysteine oxidation, *Chem. Soc. Rev.*, 2018, **47**(1), 231–268, DOI: **10.1039/C7CS00607A**.
3 H. J. Forman, J. M. Fukuto and M. Torres, Redox signaling: thiol chemistry defines which reactive oxygen and nitrogen species can act as second messengers, *Am. J. Physiol.: Cell Physiol.*, 2004, **287**(2), C246–C256, DOI: **10.1152/ajpcell.00516.2003**.
4 J. M. Denu and K. G. Tanner, Specific and Reversible Inactivation of Protein Tyrosine Phosphatases by Hydrogen Peroxide: Evidence for a Sulfenic Acid Intermediate and Implications for Redox Regulation, *Biochemistry*, 1998, **37**, 5633–5642, DOI: **10.1021/BI973035T**.
5 R. D. Michalek, K. J. Nelson and B. C. Holbrook, *et al.*, The Requirement of Reversible Cysteine Sulfenic Acid Formation for T Cell Activation and Function, *J. Immunol.*, 2007, **179**(10), 6456–6467, DOI: **10.4049/JIMMUNOL.179.10.6456**.
6 J. D. Keyes, D. Parsonage and R. D. Yammani, *et al.*, Endogenous, regulatory cysteine sulfenylation of ERK kinases in response to proliferative signals, *Free Radical Biol. Med.*, 2017, **112**, 534–543, DOI: **10.1016/J.FREERADBIOMED.2017.08.018**.
7 T. F. Brewer, F. J. Garcia, C. S. Onak, K. S. Carroll and C. J. Chang, Chemical Approaches to Discovery and Study of Sources and Targets of Hydrogen Peroxide Redox Signaling Through NADPH Oxidase Proteins, *Annu. Rev. Biochem.*, 2015, **84**(1), 765–790, DOI: **10.1146/annurev-biochem-060614-034018**.
8 E. A. Orabi and A. M. English, Sulfur-Aromatic Interactions: Modeling Cysteine and Methionine Binding to Tyrosinate and Histidinium Ions to Assess Their Influence on Protein Electron Transfer, *Isr. J. Chem.*, 2016, **56**(9–10), 872–885, DOI: **10.1002/ijch.201600047**.
9 E. A. Orabi and A. M. English, Modeling Protein S–Aromatic Motifs Reveals Their Structural and Redox Flexibility,

J. Phys. Chem. B, 2018, **122**(14), 3760–3770, DOI: 10.1021/acs.jpcb.8b00089.

10 D. Pal and P. Chakrabarti, Non-hydrogen Bond Interactions Involving the Methionine Sulfur Atom, *J. Biomol. Struct. Dyn.*, 2001, **19**(1), 115–128, DOI: 10.1080/07391102.2001.10506725.

11 M. Iwaoka, S. Takemoto, M. Okada and S. Tomoda, Weak Nonbonded S···X (X = O, N, and S) Interactions in Proteins. Statistical and Theoretical Studies, *Bull. Chem. Soc. Jpn.*, 2002, **75**(7), 1611–1625, DOI: 10.1246/bcsj.75.1611.

12 C. C. Valley, A. Cembran and J. D. Perlmutter, *et al.*, The methionine-aromatic motif plays a unique role in stabilizing protein structure, *J. Biol. Chem.*, 2012, **287**(42), 34979–34991, DOI: 10.1074/jbc.M112.374504.

13 A. R. Viguera and L. Serrano, Side-chain interactions between sulfur-containing amino acids and phenyalanine in α-helixes, *Biochemistry*, 1995, **34**(27), 8771–8779, DOI: 10.1021/bi00027a028.

14 B. J. Stapley, C. A. Rohl and A. J. Doig, Addition of side chain interactions to modified Lifson-Roig helix-coil theory: application to energetics of Phenylalanine-Methionine interactions, *Protein Sci.*, 1995, **4**(11), 2383–2391, DOI: 10.1002/pro.5560041117.

15 C. D. Tatko and M. L. Waters, Investigation of the nature of the methionine-π interaction in β-hairpin peptide model systems, *Protein Sci.*, 2004, **13**(9), 2515–2522, DOI: 10.1110/ps.04820104.

16 R. B. Best, X. Zhu and J. Shim, *et al.*, Optimization of the additive CHARMM all-atom protein force field targeting improved sampling of the backbone φ, ψ and side-chain χ(1) and χ(2) dihedral angles, *J. Chem. Theory Comput.*, 2012, **8**(9), 3257–3273, DOI: 10.1021/ct300400x.

17 W. L. Jorgensen, J. Chandrasekhar, J. D. Madura, R. W. Impey and M. L. Klein, Comparison of simple potential functions for simulating liquid water, *J. Chem. Phys.*, 1983, **79**(2), 926–935, DOI: 10.1063/1.445869.

18 A. D. MacKerell, D. Bashford and M. Bellott, *et al.*, All-Atom Empirical Potential for Molecular Modeling and Dynamics Studies of Proteins, *J. Phys. Chem. B*, 1998, **102**, 3586–3616, DOI: 10.1021/jp973084f.

19 M. J. Frisch, G. W. Trucks, H. B. Schlegel, G. E. Scuseria, M. A. Robb, J. R. Cheeseman, G. Scalmani, V. Barone, B. Mennucci, G. A. Petersson, H. Nakatsuji, M. Caricato, X. Li, H. P. Hratchian, A. F. Izmaylov, J. Bloino, G. Zheng and D. J. Sonnenb, *Gaussian 09, Revision B.01*, 2010.

20 S. F. Boys and F. Bernardi, The calculation of small molecular interactions by the differences of separate total energies. Some procedures with reduced errors, *Mol. Phys.*, 1970, **19**(4), 553–566, DOI: 10.1080/00268977000101561.

21 P. J. Stephens, F. J. Devlin, C. F. Chabalowski and M. J. Frisch, Ab Initio Calculation of Vibrational Absorption and Circular Dichroism Spectra Using Density Functional Force Fields, *J. Phys. Chem.*, 1994, **98**(45), 11623–11627, DOI: 10.1021/j100096a001.

22 Y. Zhao and D. G. Truhlar, The M06 suite of density functionals for main group thermochemistry, thermochemical kinetics, noncovalent interactions, excited states, and transition elements: two new functionals and systematic testing of four M06-class functionals and 12 other functionals, *Theor. Chem. Acc.*, 2008, **120**(1–3), 215–241, DOI: 10.1007/s00214-007-0310-x.

23 E. A. Orabi and A. M. English, Predicting structural and energetic changes in Met–aromatic motifs on methionine oxidation to the sulfoxide and sulfone, *Phys. Chem. Chem. Phys.*, 2018, **20**(35), 23132–23141, DOI: 10.1039/C8CP03277G.

24 E. A. Orabi and A. M. English, Expanding the range of binding energies and oxidizability of biologically relevant S–aromatic interactions: imidazolium and phenolate binding to sulfoxide and sulfone, *Phys. Chem. Chem. Phys.*, 2019, **21**(27), 14620–14628, DOI: 10.1039/C9CP02332A. Accessed October 10, 2019.

25 B. R. Brooks, C. L. Brooks and A. D. Mackerell, *et al.*, CHARMM: the biomolecular simulation program, *J. Comput. Chem.*, 2009, **30**(10), 1545–1614, DOI: 10.1002/jcc.21287.

26 K. Vanommeslaeghe, E. Hatcher and C. Acharya, *et al.*, CHARMM general force field: a force field for drug-like molecules compatible with the CHARMM all-atom additive biological force fields, *J. Comput. Chem.*, 2010, **31**(4), 671–690, DOI: 10.1002/jcc.21367.

27 G. Lamoureux and E. A. Orabi, Molecular modelling of cation–π interactions, *Mol. Simul.*, 2012, **38**(8–9), 704–722, DOI: 10.1080/08927022.2012.696640.

28 C. R. Rupakheti, B. Roux, F. Dehez and C. Chipot, Modeling induction phenomena in amino acid cation–π interactions, *Theor. Chem. Acc.*, 2018, **137**(12), 174, DOI: 10.1007/s00214-018-2376-z.

29 E. A. Orabi and G. Lamoureux, Cation–π and π–π Interactions in Aqueous Solution Studied Using Polarizable Potential Models, *J. Chem. Theory Comput.*, 2012, **8**(1), 182–193, DOI: 10.1021/ct200569x.

30 S. Wang, E. A. Orabi, S. Baday, S. Bernèche and G. Lamoureux, Ammonium transporters achieve charge transfer by fragmenting their substrate, *J. Am. Chem. Soc.*, 2012, **134**(25), 10419–10427, DOI: 10.1021/ja300129x.

31 E. A. Orabi and G. Lamoureux, Cation–π Interactions between Quaternary Ammonium Ions and Amino Acid Aromatic Groups in Aqueous Solution, *J. Phys. Chem. B*, 2018, **122**(8), 2251–2260, DOI: 10.1021/acs.jpcb.7b11983.

32 E. A. Orabi, R. Davis and G. Lamoureux, Drude polarizable force field for cation–π interactions of alkali and quaternary ammonium ions with aromatic amino acid side chains, *J. Comput. Chem.*, 2020, **41**, 472–481, DOI: 10.1002/jcc.26084.

33 U. Essmann, L. Perera, M. L. Berkowitz, T. Darden, H. Lee and L. G. Pedersen, A smooth particle mesh Ewald method, *J. Chem. Phys.*, 1995, **103**(19), 8577–8593, DOI: 10.1063/1.470117.

34 W. G. Hoover, Canonical dynamics: Equilibrium phase-space distributions, *Phys. Rev. A: At., Mol., Opt. Phys.*, 1985, **31**(3), 1695–1697 Accessed June 14, 2017.

35 G. J. Martyna, D. J. Tobias and M. L. Klein, Constant pressure molecular dynamics algorithms, *J. Chem. Phys.*, 1994, **101**(5), 4177–4189, DOI: 10.1063/1.467468.

36 G. J. Martyna, M. E. Tuckerman, D. J. Tobias and M. L. Klein, Explicit reversible integrators for extended systems dynamics, *Mol. Phys.*, 1996, **87**(5), 1117–1157, DOI: **10.1080/00268979600100761**.

37 S. Kumar, J. M. Rosenberg, D. Bouzida, R. H. Swendsen and P. A. Kollman, THE weighted histogram analysis method for free-energy calculations on biomolecules. I. The method, *J. Comput. Chem.*, 1992, **13**(8), 1011–1021, DOI: **10.1002/jcc.540130812**.

38 M. Souaille and B. Roux, Extension to the weighted histogram analysis method: combining umbrella sampling with free energy calculations, *Comput. Phys. Commun.*, 2001, **135**(1), 40–57, DOI: **10.1016/S0010-4655(00)00215-0**.

39 I. V. Khavrutskii, J. Dzubiella and J. A. McCammon, Computing accurate potentials of mean force in electrolyte solutions with the generalized gradient-augmented harmonic Fourier beads method, *J. Chem. Phys.*, 2008, **128**(4), 044106, DOI: **10.1063/1.2825620**.

40 E. A. Orabi and G. Lamoureux, Simulation of liquid and supercritical hydrogen sulfide and of alkali ions in the pure and aqueous liquid, *J. Chem. Theory Comput.*, 2014, **10**(8), 3221–3235, DOI: **10.1021/ct5002335**.

41 E. A. Orabi and G. H. Peslherbe, Computational insight into hydrogen persulfide and a new additive model for chemical and biological simulations, *Phys. Chem. Chem. Phys.*, 2019, **21**(29), 15988–16004, DOI: **10.1039/C9CP02998B**.

42 S. Mecozzi, A. P. West and D. A. Dougherty, Cation-pi interactions in aromatics of biological and medicinal interest: electrostatic potential surfaces as a useful qualitative guide, *Proc. Natl. Acad. Sci. U. S. A.*, 1996, **93**(20), 10566–10571, DOI: **10.1073/pnas.93.20.10566**.

43 R. Peverati and D. G. Truhlar, Quest for a universal density functional: the accuracy of density functionals across a broad spectrum of databases in chemistry and physics, *Philos. Trans. R. Soc., A*, 2014, **372**(2011), 20120476, DOI: **10.1098/rsta.2012.0476**.

44 M. Nishio, The CH/π hydrogen bond in chemistry. Conformation, supramolecules, optical resolution and interactions involving carbohydrates, *Phys. Chem. Chem. Phys.*, 2011, **13**, 13873–13900.

45 W. J. Chung, M. Ammam and N. E. Gruhn, *et al.*, Interactions of Arenes and Thioethers Resulting in Facilitated Oxidation, *Org. Lett.*, 2009, **11**(2), 397–400, DOI: **10.1021/ol802683s**.

46 N. P.-A. Monney, T. Bally, G. S. Bhagavathy and R. S. Glass, Spectroscopic Evidence for a New Type of Bonding between a Thioether Radical Cation and a Phenyl Group, *Org. Lett.*, 2013, **15**(19), 4932–4935, DOI: **10.1021/ol402126f**.

47 J. C. Aledo, F. R. Cantón and F. J. Veredas, Sulphur Atoms from Methionines Interacting with Aromatic Residues Are Less Prone to Oxidation, *Sci. Rep.*, 2015, **5**, 16955, DOI: **10.1038/srep16955**.

48 S. R. Lee, K. S. Kwon, S. R. Kim and S. G. Rhee, Reversible inactivation of protein-tyrosine phosphatase 1B in A431 cells stimulated with epidermal growth factor, *J. Biol. Chem.*, 1998, **273**(25), 15366–15372, DOI: **10.1074/jbc.273.25.15366**.

49 D. G. Ruiz, A. Sandoval-Perez, A. V. Rangarajan, E. L. Gunderson and M. P. Jacobson, Cysteine Oxidation in Proteins: Structure, Biophysics, and Simulation, *Biochemistry*, 2022, **61**, 2165–2176, DOI: **10.1021/acs.biochem.2c00349**.

50 F. R. Salsbury Jr, S. T. Knutson, L. B. Poole and J. S. Fetrow, Functional site profiling and electrostatic analysis of cysteines modifiable to cysteine sulfenic acid, *Protein Sci.*, 2008, **17**, 299–312, DOI: **10.1110/ps.073096508**.

